

Is LoRaWAN Really Wide? Fine-grained LoRa Link-level Measurement in An Urban Environment

Yidong Ren^{*†}, Li Liu^{*†}, Chenning Li^{*†}, Zhichao Cao[†], Shigang Chen[‡]

[†]Michigan State University, [‡]University of Florida

{renyidong, liuli9, lichenni, caozc}@msu.edu, sgchen@cise.ufl.edu

Abstract—Internet-of-Things (IoT) aims to connect billions of low-data rate and energy-constrained end-devices in the near future. Although many IoT systems have been commercialized, most of them focus on home and body scale applications. To establish a low-cost IoT at the city scale, LoRa Wide Area Networks (LoRaWAN) have become attractive in recent years due to their desirable kilometer or even longer communication distance with low energy consumption. However, due to the expensive cost of densely deploying end-nodes, the understanding of LoRa link behavior is still coarse-grained, and hard to fully realize the link dynamics, networking coverage, and localization accuracy of LoRaWAN in an urban environment.

This paper shows a fine-grained LoRa link-level measurement via mobile end-nodes. We deploy two gateways and six mobile end-nodes and collect data packets over four months at a $6 \times 6 \text{ km}^2$ urban area. The evaluation mainly focuses on answering three questions: 1) Does a LoRa link stably perform in both spatial and temporal dimensions? 2) How large area can be covered for reliable communication by each gateway in the urban environment? 3) What accuracy can be achieved to localize an end-node through LoRa links? According to our measurement, our key findings are 1) The spatial and temporal behavior of LoRa links is quite dynamic due to the different types of land covers and the frequent micro-environment changes in the urban areas; 2) Each gateway can cover about 11.3 km^2 area and marginal SNR gains (e.g., 2 dB) of LoRa links are efficient enough to enlarge 32.6% coverage area of a gateway; and 3). The median localization error is about 400 m. Without densely deployed LoRa gateways, the SOTA LoRa localization can support road-level localization, even when an end node is close to one of the gateways.

I. INTRODUCTION

Internet-of-Thing (IoT) is another excellent innovation after Internet and mobile networks in the information era, aiming to connect billions of low data-rate end-devices in an energy-constraint unattended manner. Among the commercial wireless techniques, Bluetooth Low Energy (BLE) is widely used in body-area networks, such as connecting wearable devices to smartphones. Wi-Fi and Zigbee can establish local-area connections like the smart home and smart building to extend the communication range further. However, all techniques mentioned above are restricted by power consumption and maintenance requirements, making it hard for wide-area and long-term deployment.

Low-power Wide Area Network (LPWAN) is an emerging IoT paradigm aiming for low-power wireless communication

over kilometer links. Several LPWANs (e.g., Long Range (LoRa) [1], Narrow-Band(NB)-IoT [2], SIGFOX [3]) with different physical layer designs have been commercialized, enabling city-scale IoT applications at a low cost. For example, NB-IoT [2] and LTE-M operate on the LTE band as a part of 5G for the massive IoT. SIGFOX [3] uses an unlicensed band but is a proprietary network. In contrast, LoRaWAN [1] operates at an unlicensed spectrum and follows an open-source standard, attracting much attention from academia and industrial communities.

LoRa networking stack adopts the Chirp Spread Spectrum (CSS) modulation at the physical layer (LoRa-PHY). By suppressing the background noise on the spectrum in CSS, LoRa-PHY can successfully demodulate a symbol even if its SNR level is as low as -20 dB [4], [5], making it a representative of the low-power and long-distance communication. With such LoRa links, spatial-temporal link dynamics, coverage, and link-information based localization are three fundamental research issues [6] which can be formulated as follows:

- For spatial-temporal link dynamics, the critical questions are whether different links with the same distance show similar link performance and whether a link's performance is stable over a long period.
- For coverage, the critical question is whether the conceptual “long-distance” can be realized in a wide area with a few LoRa gateways, enabling smart-city applications (e.g., vehicle sharing [7], environment monitoring [8], [9], metering, logistics)?
- For link-information based localization, the critical question is whether an end-node can be accurately localized with LoRa link fingerprint in a wide area and sparse deployment.

With the answers to these questions, a fine-grained link-level measurement can benefit the deployment of LoRa gateways, service quality in mobile applications, and network management in practice.

Status Quo and their Limitations: Several works [10]–[12] have observed the spatial diversity of LoRa links, but lack detailed analysis in different distance scales. To our best knowledge, no work reports the temporal performance of LoRa links. Similarly, to answer the coverage question, some measurement studies [7], [13]–[18] deployed real LoRaWAN systems to study the coarse-grained communication range in real environments. For example, Liando et al. [13] deployed

^{*}Indicates equal contribution

three LoRa gateways and more than 50 static LoRa end nodes in a $3 \times 3 \text{ km}^2$ campus environment to conduct a coverage measurement. And they further use a 70% packet delivery ratio (PDR) as a threshold to approximate the communication range of a LoRa link. The results show that the maximum communication range is 9.08 km and 2 km in Line-of-Sight (LoS) and Non-Line-of-Sight (NLoS) scenarios. However, with only a communication range, the communication heterogeneity [11], [19] will cause significant uncertainty in the coverage area for a gateway. Thus, the coverage problem is not fully addressed.

Compared to the energy-consuming GPS-based localization, LoRa link fingerprint based localization consumes much less power at the expense of accuracy. To answer the localization question, the SOTA LoRa localization method, SateLoc [20] reported a median localization error of 43.5 m in a $350 \times 650 \text{ m}^2$ urban area with three gateways. However, the size of the evaluated area is limited, and the cost of dense gateways deployment is unaffordable. Thus, whether we can achieve the same localization accuracy in a larger area and with sparsely deployed gateways is still questionable.

Challenges: To achieve fine-grained spatial-temporal dynamics, coverage, and localization measurement, the key information is to obtain the link PDR and signal fingerprint at a fine-grained geography scale. We take a $6 \times 6 \text{ km}^2$ area as an example to demonstrate the difficulty of obtaining such information. If we split the whole area into 100 m^2 (i.e., the geography scale) cells and deploy a LoRa end node in each cell, 3,600 LoRa end nodes are required. The number of LoRa end nodes increases as the geography scale becomes more fine-grained. The expensive cost makes a static deployment impossible to achieve the fine-grained link-level measurement.

In this paper, we deploy a mobile LoRaWAN system and propose novel methods to measure the LoRa link-level coverage area and localization accuracy in a wide urban area at a fine-grained geography scale. Our deployed mobile LoRaWAN system consists of two LoRa gateways and six mobile LoRa end nodes in a $6 \times 6 \text{ km}^2$ urban area, which continuously transmits data packets with the location information while they are moving. Although benefiting from the mobility of the LoRa end nodes, thousands of LoRa links are recorded efficiently, covering a variety of different locations, we still encounter two challenges to achieve the fine-grained and whole-area measurement. On the one hand, since a LoRa end node keeps moving, it needs time to observe enough packets for PDR calculation, but it travels for a distance as well. Such mobility leads to a granularity tradeoff between the PDR calculation and the geography scale. On the other hand, the users carrying the mobile end nodes moved freely in their daily life, without any requirement for movement. Thus, the locations of the collected data are not uniformly distributed across the areas of interest. Although we have available data records over four months, some locations and roads are still uncovered. In such areas, it is not trivial to infer the coverage performance and establish a fingerprint map for localization.

To solve the first challenge, The PDR granularity indicates the PDR estimation precision we can achieve by observing

different numbers of packet transmissions. The more packets we count, the higher the precision is. For example, the precision will be 0.1 if we only count 10 packets in total, but it will be 0.01 if 100 packets are counted. We estimate the speed of each LoRa end node (§III-C), then adaptively adjust the geography scale to ensure the PDR granularity is not higher than 0.1 (§IV-A). Moreover, we adopt DeepLoRa [11] to generate the expected signal power (ESP) [10] for every location in the area. DeepLoRa [11] is a deep neural network (DNN) based ESP estimation model to predict accurate ESP values by taking a land-cover type sequence as input. For coverage, with the calculated PDRs in the covered locations, we establish an ESP based PDR prediction model to infer the PDRs in the uncovered locations (§IV-E). For localization, we use the ESPs observed by different gateways as fingerprints to generate a fingerprint map for each location.

With the ESP, PDR, and fingerprint map, our link-level measurement includes the following aspects. First, with the ESPs and PDRs in the covered locations, we analyze the overall, spatial and temporal link dynamics for link property analysis (§IV-C and §IV-D). Second, we estimate the coverage area of each gateway with/without link ESP gains (§V). Third, we study the localization accuracy with the fingerprint map under various settings (§VI). Our measurement study presents three key observations, and the conclusions are as follows:

- The distance cannot reflect the link quality anymore, and the temporal link behavior is much more dynamic due to the micro-environment changes.
- Although the maximum communication range of a gateway observed by us is over 3 km, its actual coverage area is irregular and only about 11.3 km^2 , which is much less than expected.
- The fingerprint-based LoRa localization accuracy is quite limited in sparse gateway deployment. More gateways, site-survey, and dynamic calibration are needed.

We summarize our contributions as follows:

- We deploy a real mobile LoRaWAN system in an urban area and measure massive LoRa links over four months. The dataset is available ¹ and will inspire more fine-grained studies of LoRaWAN than state-of-the-arts [7], [13]–[18].
- We propose several methods to measure spatial/temporal link dynamics and enable coverage area calculation using sparsely received LoRa packets.
- We report the localization accuracy in such a wide-area deployment providing more insights for future localization method design in LoRaWAN.

II. RELATED WORK

LoRa Link Dynamic Study. To estimate the coverage of LoRa gateways without the deployment and on-site measurements, Demetri et al. [10], SateLoc [20], and DeepLoRa [11] develop different models to accurately estimate the signal path

¹Codes and datasets can be found on GitHub: https://github.com/lilygeek/LoSee_ICNP

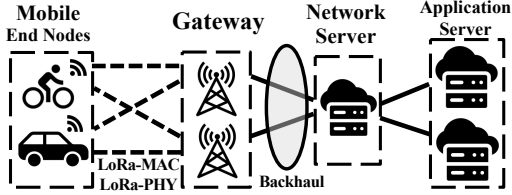


Fig. 1: Illustration of our LoRaWAN architecture.

loss by understanding the impact of land-cover types in an urban environment. And a variety of remote sensing techniques are adopted to recognize land covers through the LoRa link. For example, Demetri et al. [10] first design an automated processing toolchain with the multi-spectral images from remote sensing and then apply the Okumura-Hata formula [21] for path loss prediction. Similarly, SateLoc [20] proposes a segmented Bor model [22] to capture the different path loss exponents with corresponding land covers. DeepLoRa [11] further incorporates the deep learning techniques for LoRa link estimation. It develops a land-cover aware path loss model based on the Bi-LSTM (Bidirectional Long Short Term Memory) and reduces the estimation error to less than 4 dB, which is $2\times$ smaller than state-of-the-art models [10]. In contrast, we study the relationship between a path loss and the resulting PDR, which is crucial in bridging the gap between link behavior and network coverage.

LoRa Coverage Measurement. Recent years have witnessed several measurement works [3], [7], [12], [13], [23]–[25] to reveal the LoRaWAN performance in real environments. Liando et al. [13] deploy three gateways and more than 50 static end nodes in a $3\times 3\text{ km}^2$ campus to study the LoRaWAN performance for measurement, including the communication range, network throughput, and energy efficiency. Results show that the LOS and NLOS communication ranges are 9.08 km and 2 km, respectively. Similarly, Centenaro et al. [3] observe a communication range of 2 km in an area of high buildings. And the communication range they reported varies from 1 km to 20 km in the central business district [24]. Besides, LoSee [7] adopts a mobile end node mounted on a bike to study the LoRaWAN coverage ability on the campus scale (e.g., 4.5 km^2). For reliable PDR calculation, the mobile end node must transmit 50 to 100 packets on the spot. Focusing on the indoor environments (e.g., office buildings, residential buildings, car parks, warehouses), Xu et al. [23] study the LoRa link behavior and energy profile by deploying ten static and two mobile LoRa end nodes. Compared to these measurement studies only focusing on the spatial link behavior, we analyze the temporal characteristics of LoRa links and provide a more fine-grained coverage area study than existing works in a $6\times 6\text{ km}^2$ urban area.

LoRa Localization Method. Studies mainly adopt two kinds of technologies for LoRa localization: 1) TDoA-based localization; 2) RSSI-based localization. TDoA-based approaches utilize the time differences of the same signal arriving at different gateways. TDoA has been implemented in the Lo-

RaWAN network to perform localization both for stationary [26] and mobile scenarios [27]–[29]. However, due to the limited bandwidth of commercial LoRa end nodes, TDoA-based localization error can reach hundreds of meters since only μs -level time resolution [30], [31] can be achieved. Researchers have improved TDoA-based localization to meter-level by customizing dedicated LoRa devices. Nandakumar et al. [32] proposed a multi-band LoRa backscatter device based on CSS modulation. Bansal et al. [33] present a distributed software-radio-based station network that spans a wide bandwidth encompassing the TV whitespaces and offers a high aperture. Those approaches, however, cannot be applied directly in existing LoRaWAN systems. Besides, TDoA-based systems require at least three gateways that are strictly time-synchronized or phase-synchronized which is not applicable in scenarios with sparse gateway deployment.

We can utilize received signal strength indicator (RSSI) measurements for localization [34] according to the path loss models mentioned above [22], [35]. However, the performance is highly affected by channel dynamics in complicated environments [10], [11], [20]. Fingerprint-based approaches [36]–[39] also use RSSI values as a fingerprint to locate an end node by matching its fingerprint with known reference locations in the database. Machine learning approaches have been adopted for fingerprint matching, such as k-Nearest-Neighbor (KNN) [37], SVM [36], Bayesian inference [38], [39]. SateLoc [20] proposes a weighted combination strategy for multi-gateway likelihood maps based on fingerprint matching and selects the point with the highest likelihood as the predicted location. SateLoc achieves a 43.5 m median localization error in a 227,500 m² urban area. Based on our LoRaWAN setting, we adopt link RSSI localization which is similar to SateLoc and provide a detailed localization comparison with the data collected from our mobile LoRa system.

III. SYSTEM AND DATASET OVERVIEW

In this section, we first briefly review the LoRaWAN technical specification and define the LoRa coverage problem. An overview is then given on the system architecture, configuration, and deployment. Finally, we show the measurements and analysis results from our deployed mobile LoRa system.

A. LoRaWAN Primer

We illustrate the architecture of LoRaWAN in Figure 1 which operates in the infrastructure mode. Multiple LoRa end nodes run the LoRa-MAC (media access control) and LoRa-PHY protocols and connect to the gateways in their communication range. Transport protocols like TCP, 6lowpan, and COAP is not involved in the LoRaWAN networking stack yet. Hence, we mainly focus on the link layer performance. Upon receiving the LoRa packets, gateways forward them to LoRa network servers for further processing. Note that there is no energy constraint on the gateway in most scenarios [5], [40]. Since the connection between gateways and network servers are usually cellular networks or wired networks. As the packet forwarder, gateways also forward the control messages (e.g.,

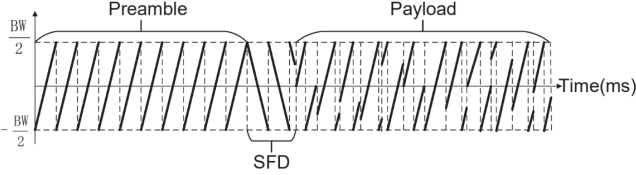


Fig. 2: The structure of a LoRa packet.

PHY configurations, MAC settings) from network servers to end nodes. Finally, network servers filter duplicated LoRa packets and disseminate the valid ones into application servers for different applications.

As for LoRa networking, LoRa-PHY uses CSS to modulate data symbols. Figure 2 shows the structure of a LoRa packet, which consists of the preamble, start frame delimiter (SFD), and payload. Specifically, the preamble consists of multiple base up-chirps, followed by the SFD with 2.25 base down-chirps for packet detection and alignment. The payload contains multiple modulated chirps with different shifted initial frequencies for encoded data bits. In LoRa-PHY, three parameters (i.e., bandwidth (BW), spreading factor (SF), and coding rate (CR)) can be configured to adapt the communication range. For example, BW determines the frequency range of a chirp symbol, such as 125, 250, and 500 kHz, in which a small BW corresponds to an extensive communication range [5]. SF denotes the data bits a chirp symbol represents, ranging from 7 to 12. The communication range gets larger as the SF increases and enhances the noise resilience of LoRa signals. Besides, CR introduces data redundancy in the coding process for extra noise tolerance, which can be assigned as 4/5, 4/6, 4/7, and 4/8.

Sitting upon LoRa-PHY, LoRa-MAC adopts an ALOHA-based protocol that allows end nodes to transmit as soon as they wake up, and exponential back-off is involved in case of collisions. However, ISM bands regulation imposes a maximum 1% transmission duty cycle to end nodes and gateways when using an ALOHA MAC. As a result, it puts a significant limitation on the downlink capacity of the gateways as they need to serve all the surrounding end nodes with relatively scarce transmission opportunities.

B. Our System Overview

We first introduce the hardware and deployment of our mobile LoRaWAN system. Illustrated in Figure 3, two gateways G_1 and G_2 and six mobile end nodes (e.g., bicycle, car) are deployed in the $6 \times 6 \text{ km}^2$ urban area. Both gateways are equipped with an MCU, an SX1276 transceiver [4], and a Raspberry Pi 3 for programming remotely. We further indicate the location of our two gateways G_1 and G_2 in the campus as white points in Figure 3(a), which are located at the rooftop of two different buildings at the height of 84 m and 68 m, respectively. Note that the ground altitude of the campus area is about 52 m, and the distance between G_1 and G_2 is 1332.14 m. The gateways are powered by PoE (Power over Ethernet) and provided with Internet access. Thus it can

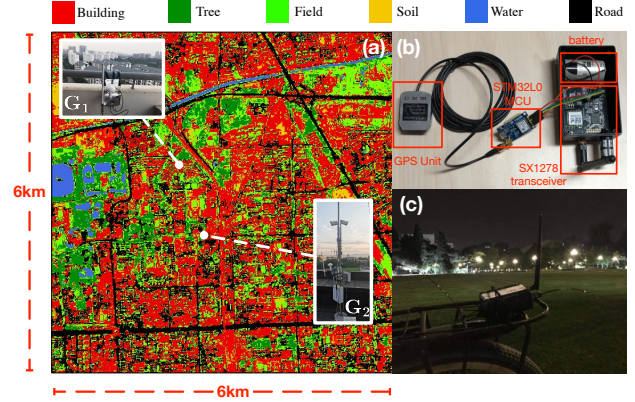


Fig. 3: We deploy two gateways and six mobile nodes in the urban areas, covering various land cover types.

forward the LoRa packets to our network and application servers running on the cloud (e.g., Digital Ocean).

On the transmitter side, the LoRa end nodes are implemented with an MCU, an SX1278 transceiver, and a GPS unit, as shown in Figure 3(b). Figure 3(c) illustrates the 5 LoRa end nodes mounted on different bicycles, and the remaining end node is put inside a BYD car under the front windshield glass. These end nodes move freely with the bicycles/car in the users' daily life without any constraints, they send a packet to the gateways every five seconds only when they are moving for power efficiency.

By default, our experiment uses the spreading factor $SF = 12$, bandwidth $BW = 125 \text{ kHz}$, and coding rate $CR = 4/5$. We enable a regulation-compatible power amplifier controlled by the register PA_HP [4] and connected to the pin PA_BOOST [4] on the SX1278 transceiver. The total transmission power reaches 19 dB, which complies with LoRa regulations. The operating channel is set as 486.3 kHz, 486.5 kHz, 486.7 kHz, 486.9 kHz, 487.1 kHz and 487.3 kHz, respectively. Thus we can avoid potential packet loss due to collisions between different end nodes. The experiment spans four months, during which the end node owners traveled as usual (e.g., eating, office, home). Thus the collected data records can only cover several parts of the whole area. To obtain the land-cover types in this area for the LoRa based localization, we apply the satellite remote sensing imaging on the whole area of interest by following the instructions in existing works [10], [11], [20], including buildings, roads, parking lots, lakes, a river, grassland, trees, and playground.

C. Collected Dataset Overview

This section provides detailed instruction on our collected LoRa dataset, spanning from Dec 22 to Mar 15. Considering the fast movement of an end node, the transmission interval between two adjacent packets is set as 5s. We encode the GPS coordinates, timestamps, and sequence numbers into the payload of LoRa packets. And the corresponding SNR and RSSI are logged at the gateway side. Upon receiving the packets, the logged data records can be extracted from

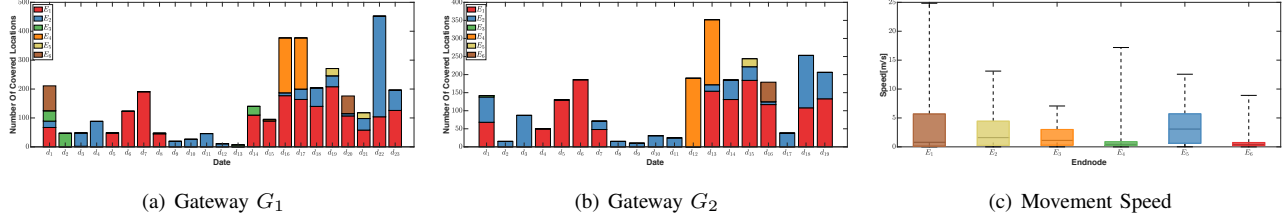


Fig. 4: The accumulated number of different locations observed by (a) G_1 and (b) G_2 across different users on different days. (c) Movement speed distribution of six mobile end nodes.

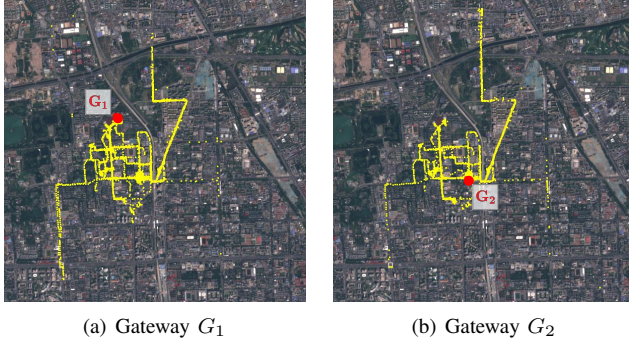


Fig. 5: The spatial distribution of data records in the view of G_1 and G_2 .

the network server to keep the duplicate packets at both gateways, delivering over 30,000 records in total. Besides, we can calculate the link distance and the height difference between the end node and gateway pair by decoding the GPS data in the payloads.

We further illustrate the measuring locations on the main roads of the $6 \times 6 \text{ km}^2$ urban area, shown in Figure 5. The yellow points and red ones indicate the moving end nodes and the gateway G_1 and G_2 as the receivers for successful packet transmissions. And the maximum communication range of G_1 and G_2 can be larger than 3 km . Additionally, we observe similar trajectories of end nodes for G_1 and G_2 , but the PDR of an identical road is quite diverse. For example, both G_1 and G_2 have poor performance on the right-center roads in common. However, G_1 has better coverage for the left-bottom road while G_2 performs better on the middle-top road, especially the part in the north of a river on the top. The observation shows that the maximum communication range is too coarse-grained to understand the coverage of LoRaWAN in an urban area, and a finer-grained report on the measurement of LoRaWAN is required.

To demonstrate the coverage of both gateways statistically in our mobile LoRa system, we show the total number of covered locations with successful transmissions in terms of end nodes and days, shown in Figure 4. Specifically, we use a $10 \times 10 \text{ m}^2$ square block to define our “locations”. Thus the whole area can be divided into 600×600 locations. For each end node, we calculate the total number of various trajectories with corresponding transmitting locations. For example, if more than one packet is received in a new location, we count

once for the current end node and derive the total covered locations. Figure 4(a) and 4(b) show that the covered locations by G_1 on 23 different days, while G_2 observes data for 19 days. Regarding the successful transmissions for each day, the maximum and minimum locations observed by G_1 are 452 and 7. In contrast, G_2 's maximum and minimum observed locations are 352 and 10, respectively. From the view of mobile end nodes, end nodes 1 (e.g., red) and 2 (e.g., deep blue) contribute the most data records in different locations on most days. And other nodes demonstrate a varied covered location. For example, end node 4 (e.g., orange) only delivers the most covered locations in two days.

To measure the mobility of our end nodes, we further calculated the speed of each end node by using the timestamps between two adjacent locations in a trajectory. The speed distributions (i.e., min, 25%, median, 75%, and max) of different end nodes are shown in Figure 4(c). The maximum observed speed is about 25 m/s (90 km/h) from the end node 1 (i.e., the BYD car). The median speed is less than 5 m/s (18 km/h) for most nodes, which is reasonable for a bicycle. Note that data records related to end node 1 are taken during the morning and afternoon traffic peak hours. Since LoRa-PHY is resilient to the Doppler effect [13] in the range of our observed speed, we can use these data records to estimate an equivalent PDR for different locations for transmitting nodes.

IV. LINK BEHAVIOR STUDY

Given our collected dataset with mobile LoRa nodes, we study the LoRa link behavior in the urban area. Two metrics, ESP and PDR, are adopted to indicate the signal path loss over a physical channel and reliable coverage in an area. By carefully analyzing their spatial and temporal distributions, we establish a PDR prediction model that associates a position's computed ESP value to the estimated PDR.

A. Estimation Methodology on Metrics

ESP Estimation. We use ESP to depict the LoRa signal attenuation over a long-distance transmission. Although RSSI is a widely adopted indicator to measure the signal attenuation of a physical link in WSNs [41]–[43] and Wi-Fi [44], it can be more error-prone below the noise floor in LoRaWAN. Thus, we choose ESP which combines RSSI and SNR to calibrate

the expected signal path loss in our measurement study, which be calculated as follows [11], [37]:

$$\text{ESP} = \text{RSSI} + \text{SNR} - 10 \log_{10}(1 + 10^{0.1\text{SNR}}) \quad (1)$$

where RSSI is the received signal strength indicator, and SNR is the signal-to-noise ratio. Given a received data packet, its RSSI and SNR will be automatically calculated by gateways forwarded to the network server.

PDR Estimation. Given a PDR threshold, the PDR of nodes with each position can be used to determine the coverage of our mobile LoRa system. Due to the mobility of the end nodes, the data packets are scattered along various trajectories. Our basic idea is to utilize all trajectories that pass the position based on their coordinates to calculate the PDR of a specific position.

Given this trajectory-based PDR estimation method, a trade-off should be considered between the position granularity and the estimation accuracy. On the one hand, a fine-grained position granularity is desirable so that the micro-differences can be reflected across the observed “positions” by our mobile end nodes. On the other hand, the number of available trajectories can be reduced for observed locations if we split the urban area at a highly finer-grained scale to represent a position. Consequently, the PDR accuracy of mobile end nodes can suffer from the estimation bias from limited trajectories. For example, assuming the true PDR of a position is 90%, the calculated PDR is only 80% due to one packet loss of five observed packets. More than ten packet records are required for each position to mitigate the scarce trajectory distribution.

In practice, we first divide the $6 \times 6 \text{ km}^2$ area into 1,600 $150 \times 150 \text{ m}^2$ square blocks. Each block represents a position denoted as $p(i, j)$ to balance the estimation granularity and the estimation error, where i and j are the coordinates of the corresponding block. Assuming the average speed of an end node is 3 m/s from Figure 4(c), the packet interval between two adjacent transmissions is set as 5 s . Thus the end node can travel through 150 m for ten continuous packet records.

Upon receiving the LoRa packets at the gateway side, we first extract all trajectories for each end node. Then, we estimate all n positions that a trajectory t covers. For the k^{th} position $p_t(k)$ of trajectory t , we use the sequence numbers of the data records to count the total number of transmitted LoRa packets passing through the current position, denoted as $c_t(p_t(k))$. And the number of successfully received LoRa packets is denoted as $c_r(p_t(k))$. The trajectory t only contributes a valid PDR estimation as $c_r(p_t(k))/c_t(p_t(k))$ for the position $p_t(k)$ when $c_t(p_t(k))$ is larger than 10. When we traverse all trajectories to compute their PDR estimations for the covered positions, we calculate the average value with all PDR estimations for each position.

Furthermore, we adaptively enlarge the splitting area of a position where the observed packet is less than five but not 0. Specifically, if the total number of packet transmissions is less than 5 for position $p_t(k)$, we keep increasing the area of the position by adding its adjacent blocks until more than 5 data

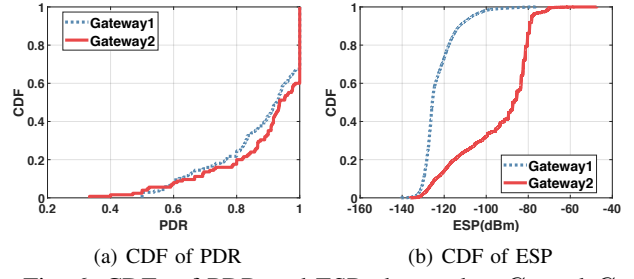


Fig. 6: CDFs of PDR and ESP observed at G_1 and G_2 .

records are reported. For G_1 , the blocks of packets less than 5 take 12.16% of all the blocks number. For G_2 , the blocks of packets less than 5 take 12.97%. In this way, we deliver a reliable PDR estimation for those covered positions with one or two lossy trajectories (e.g., the right-middle roads for G_1 and G_2 in Figure 5).

B. Overall PDR and ESP Distribution

We further demonstrate the estimated PDR and ESP across different positions for G_1 and G_2 . Illustrated in Figure 6(a), the CDFs of PDR are distributed similarly for G_1 (e.g., blue dashed curve) and G_2 (e.g., solid red curve). In comparison, G_1 provides a little better PDR for the covered positions than G_2 does. And 60% of links are reliable with a PDR higher than 90% for G_1 . And the remaining 40% LoRa links are intermediate links with dynamic link behaviors.

Figure 6(b) further shows the CDFs of ESP in all recorded data packets. We can observe that the minimum ESP is -142.3 dBm for all packets, which is consistent with the reported -148 dBm for the sensitivity of SX1276 [4]. Notice that LoRa gateways with different transceiver types definitely receive signals at different sensitivity levels, resulting in a varied link budget. Compared with G_1 , the ESP observed at G_2 is much higher. For example, G_1 has 20% ESP higher than -120 dBm and the maximum ESP is -80 dBm . However, 80% ESP of G_2 is higher than -120 dBm , and the maximum ESP is approaching -47.34 dBm . As shown in Figure 3(a), we attribute the ESP difference to the deployment environment. G_1 ’s antenna is partially hidden by the wall and railing while there is no obstacle for G_2 .

Remark. Figure 6 reflects the distribution inconsistency between PDR and ESP. Due to the strong noise tolerance ability of LoRa, low ESP (e.g., median value -127 dB) can achieve similar PDR distribution as high ESP (e.g., median value -87 dB) does.

C. Spatial PDR and ESP Distribution

We study the spatial distribution of PDR and ESP regarding the link distance. For each position (e.g., $150 \times 150 \text{ m}^2$ block), the distance between the center of the block to a gateway location is first calculated as its distance. And we use the GPS coordinates to compute the distance between the end node and a gateway for each data packet. The spatial PDR distribution is shown in Figure 7. A similar spatial distribution can be observed at G_1 and G_2 , where the intermediate links

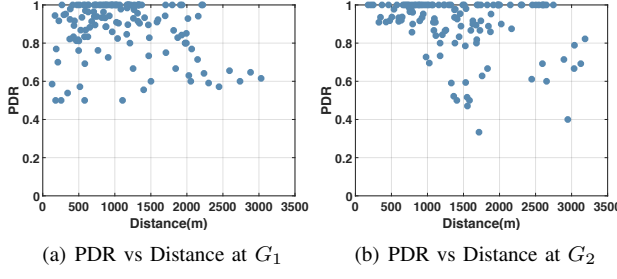


Fig. 7: The spatial distribution for PDR and distance.

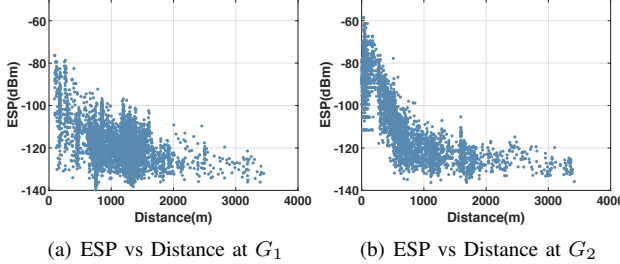


Fig. 8: The spatial distribution for ESP and distance.

with low PDR are scattered at all distance levels. We further illustrate the spatial ESP distribution in Figure 8. As the distance increase, the ESP values are reduced for both G_1 and G_2 and scattered in a relatively wide range at different distance levels. Specifically, the maximum range of ESP values is from -140 dBm to -95 dBm at G_1 in Figure 8(a) when the distance is about $1,000 \text{ m}$. In contrast, it is from -139 dBm to -100 dBm for G_2 in Figure 8(b). Additionally, the longest distance observed by ESP is about 3.5 km , which is longer than 3.2 km observed by PDR. The main reason is that the data records reported at those long-distance positions are from the end node 1 (i.e., the car). And it becomes hard to observe enough data records in our defined position area due to the high mobility, resulting in a failed estimation of PDR in long-distance areas.

Remark. The distance of a LoRa link is weakly associated with its PDR and ESP. A rough estimation of ESP can be given with the link distance (Figure 7), but the link distance cannot be used for fine-grained PDR prediction (Figure 8).

D. Temporal PDR and ESP Distribution

The temporal distribution of PDR and ESP is evaluated for transmission days. We first associate the trajectories per day to each position and then compute the standard deviation of per-day PDR values to depict the temporal PDR changes for each position. As for ESP, we first divide the whole area into $360,000 10 \times 10 \text{ m}^2$ blocks and then calculate the average ESP of the associated data records to represent the ESP of the block. The standard deviation of ESP values can be further derived for each block.

We show the CDFs of PDR and ESP deviation in Figure 9(a) and 9(b) respectively. On the one hand, G_1 and G_2 exhibit analogous temporal deviation on PDR and ESP. For example,

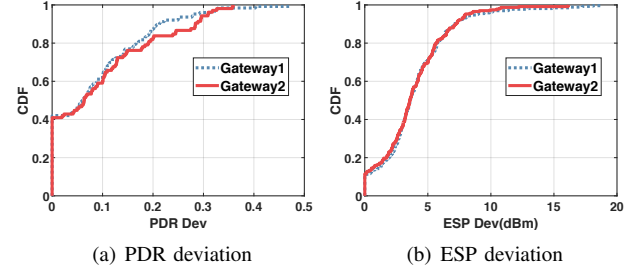


Fig. 9: The standard deviation of ESP and PDR observed on different days.

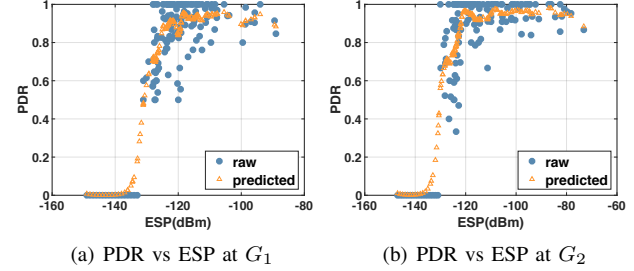


Fig. 10: Gaussian process regression analysis between PDR and ESP at G_1 and G_2 .

30% of positions have more than 5 dB variance for ESP. And the maximum ESP deviation is about -15 dB . Besides, more than 10% variances of PDR are reported for 40% of positions. And the maximum PDR deviation is larger than 30%. On the other hand, the only difference in temporal distribution over time is from the micro-environment (e.g., surrounding obstacles like other bicycles and cars), demonstrating the significant impact of the micro-environment patterns on the link performance for different end nodes.

Remark. LoRa links are highly dynamic over time in an urban environment, shown in Figure 9, which can be attributed to the frequently varying micro-environment [12].

E. ESP based PDR Prediction

Based on the above observations on PDR and ESP distributions, we build a PDR prediction model by feeding ESP as input. First, we calculate the average ESP of all observed data records for each associated position in the urban area. Given the measured PDR for covered areas, we obtain a variety of pairs of PDR and ESP. Then, the Gaussian process regression (GPR) [45] is adopted to predict the numerical PDR from ESP for those uncovered areas.

To achieve a more accurate regression learner, we choose the exponential function as the kernel function and complete the fitting processing, shown in Figure 10. Statistically, the root-mean-square error is 0.12448 and 0.13678 for G_1 and G_2 , and the coefficient of determination is 0.84 and 0.82, respectively. From the raw data pairs (e.g., blue dot), when ESP is lower than -133 dBm and -131 dBm for both gateways, the measured PDR nears 0 based on our measurement study. Additionally, a 11 dB wide transition zone (i.e., $[-131 \text{ dBm},$

-120 dBm) can be observed in both G_1 and G_2 , which is larger than a 3 dB transition zone in WSNs [43]. The reason is that in LoRa long-distance communication, LoRa links are affected by more complicated factors and are less predictable with only ESP, thus introducing more ambiguity. Even when the ESP is larger than -120 dBm , the PDR achieves a high performance but is not always 100%. And it can decrease below 70% due to a large temporal variance of PDR and ESP observed in § IV-D. As for the uncovered areas with the given ESP, the predicted data points (e.g., yellow triangle) exhibit a good match with the ground truth. However, it cannot reflect the dynamic PDR accurately in our mobile LoRa system.

Remark. ESP is a relatively good indicator to predict the PDR of a position. A 13 dB transition zone and the PDR dynamic under large ESP indicate LoRa links are less predictable than other wireless techniques like Wi-Fi and Zigbee.

V. COVERAGE AREA STUDY

A. LoRa Coverage Problem

The coverage area indicates where a gateway can reliably communicate with any end node and is determined by LoRa-PHY and LoRa-MAC. The influence of LoRa-PHY on coverage is explicit. LoRa-PHY determines a signal-to-noise ratio (SNR) threshold, under which LoRa chirp symbols cannot be decoded correctly. The SNR thresholds are determined by different LoRa-PHY configurations [5]. The observed ESP of various LoRa links is related to their distance. Thus, LoRa-PHY determines the link reliability for LoRa transmissions.

Besides, LoRa-MAC may influence the coverage, too. For example, LoRa-MAC determines collision probability when multiple LoRa end-nodes are deployed in the same area and share an identical gateway. WiChronos [46] reported that when an end node transmits a 1-byte message every ten minutes, the collision probability is about 1.4% for 100 nodes, increasing to 12.75% for 1000 nodes. However, the influence of collision on the coverage is implicit since the collision is not determined by link distance but by the transmission schedule. If the schedule is not well adjusted, the end nodes far from the gateway may not have a higher collision probability than the end nodes near the gateway even if the transmission of the far end nodes is using a longer signal on-air time (e.g., larger spreading factor). Therefore, if the transmission schedules of all end-nodes are uniformly random, the collision will uniformly degrade the transmission reliability for long and short links, making it stained for part of the LoRa-PHY covered area. Many works [40], [47] focus on solving the collided LoRa signals to enhance the LoRa transmission reliability.

In our measurement work, we focus on the LoRa-PHY coverage to determine the maximum area a LoRa gateway can cover. By adjusting the channel of each mobile end node to a different frequency [III-B], there is no signal collision in our collected datasets.

B. Methodology and Implementation

In this section, we study the coverage of each gateway in our deployed mobile LoRa system. And the coverage area is

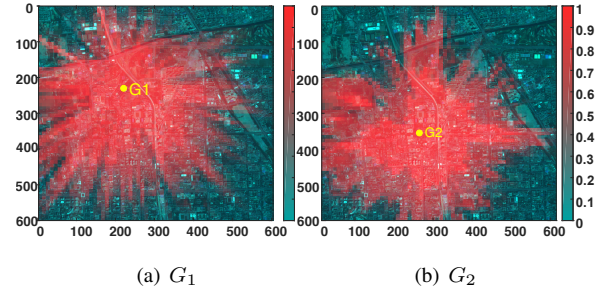


Fig. 11: The heatmap of PDR values for different positions in the urban area.

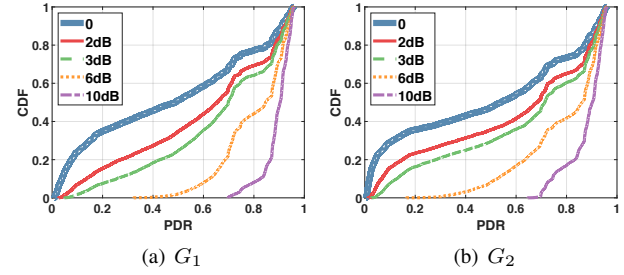


Fig. 12: CDF of predicted PDR with different ESP gains.

defined as the covered area whose sum of the positions with a PDR value larger than 70%. Specifically, by dividing the urban area into “positions” ($150 \times 150 \text{ m}^2$), we first compute the corresponding PDR with our data records for those covered areas. We first adopt DeepLoRa [11] to estimate an average ESP for each position for those uncovered ones. Then, we can predict the associated PDR based on the PDR-ESP regression model in § IV-E. Figure 11 illustrates the distribution of calculated and predicted PDR values for all positions in the urban areas. We can observe an irregular PDR distribution in different directions for both G_1 and G_2 . And the covered positions for G_1 and G_2 are distributed non-uniformly. Statistically, the coverage area of G_1 and G_2 is 11.4 km^2 and 11.6 km^2 , respectively, far from covering all $6 \times 6 \text{ km}^2$ reliably.

C. Coverage Improvement ESP Gain

To enhance the coverage area of each gateway in the wild, several systems [38], [48], [49] have been proposed to cooperate with multiple gateways for extra SNR gains of received LoRa signals. For example, an SNR gain of $2 \sim 3 \text{ dB}$ can be achieved through the coherent combining across three or more gateways [38], [48]. Equation 1 shows the SNR gain is equivalent to the ESP gain. To quantitative the relationship between the ESP gains and the coverage area in our deployed system, we manually add an ESP gain for each position and then recalculate the corresponding PDR under the enhanced ESP. For fairness, different ESP gains from 2 dB to 10 dB are selected randomly, resulting in the CDF of predicted PDR in Figure 12. As the extra ESP gains go up, the PDR increases as well. For example, the median PDR improvement can reach 48.6% to 62.8% at G_1 with a 3 dB ESP gain, shown in Figure 12(a). And it gets larger from 50.3% to 62.7% when

TABLE I: Coverage area under different ESP gains.

ESP Gains (dB)	0	2	3	6	10
G_1 Coverage Area (km^2)	11.4	15.2	17.7	27.1	35.9
G_2 Coverage Area (km^2)	11.6	15.3	17.3	23.7	33.0

the ESP gain is $10\ dB$, delivering a covered area with all PDR values larger than 70%. The observations in Figure 12 verify the effectiveness of the SNR enhancement method.

Illustrated in Table I, we further adopt the enhanced PDR to calculate the coverage area. And a steady improvement of the coverage area can be observed at G_1 and G_2 as the ESP gains increase. Given the $2\ dB$ ESP gains, the coverage area can be increased by 32.6%. And we can approximately cover the whole urban area of $6 \times 6\ km^2$ via only one gateway, with a given ESP gain of $10\ dB$.

Remark. Due to the observed link dynamics, the coverage area of a gateway is usually irregular. Beyond deploying new gateways, it can be more effective to enlarge the coverage area of a gateway by capturing extra SNR gains of LoRa signals.

VI. LOCALIZATION ACCURACY STUDY

A. Methodology and Implementation

Recent years have witnessed a variety of localization systems [7], [11], [20], [50]–[53] built on the knowledge of LoRa link behaviors with path loss. Among them, SateLoc [20] is the SOTA method. The basic method is illustrated as follows: Suppose we have several gateways to cover a certain area for localization. Each gateway will generate an ESP map as a part of the fingerprint map. The whole area is split into many geography cells, which indicate the location unit in the localization process. Given the m^{th} gateway's ESP map, the likelihood of $L_{m,i}$ for the i^{th} cell that an end node e is located can be formulated as follows:

$$L_{m,i} = \frac{|\bar{E}_{m,e} - E_{m,i}|}{\max(|\bar{E}_{m,e} - E_m|) - \min(|\bar{E}_{m,e} - E_m|)} \quad (2)$$

where $\bar{E}_{m,e}$ is the average ESP value of each packet, which is transmitted by the end node e and received at the m^{th} gateway. $E_{m,i}$ is the ESP value predicted by path loss models at the i^{th} cell in the m^{th} ESP map. The likelihood is then scaled and normalized according to the value range of differences between received and ESP values in the m^{th} ESP map. Given the likelihood map for each gateway, the fingerprint-based localization leverages the joint likelihood of multiple gateways, in which the cell with the highest likelihood is selected as the predicted location:

$$\text{Location} = \arg \max_i \sum_{m=1}^M L_{m,i} \quad (3)$$

To evaluate the performance of LoRa link-based localization systems in our deployment, we implement SateLoc based on four different path loss models for ESP map generation, including Bor model [22], PATH/INTERSECTION [10],

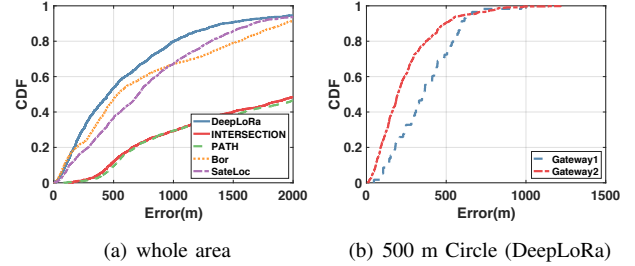


Fig. 13: The CDF of localization errors under different ESP estimation methods in different ranges.

SateLoc [20] and DeepLoRa [11]. To obtain the remote sensing images for the environmental analysis for PATH/INTERSECTION, SateLoc, and DeepLoRa, we first use the Sentinel-2 open-access API to get multi-spectral images of $10\ m$ resolution for all four path loss models. The models are then trained with the collected dataset in our deployed system, delivering 2 ESP maps for both gateways. Each pixel in our ESP map corresponds to a $10 \times 10\ m^2$ cell in a real map. Note that the evaluated data points are filtered from the whole dataset, in which each packet record contains the ESP values of the same frame from the end node received at two gateways. Finally, we collected available data records covering 1,495 different $10 \times 10\ m^2$ locations.

B. Overall Comparison of Localization Accuracy

Illustrated in 13(a), the CDF of localization error is given for the comparison study of localization accuracy. On our dataset, with the most accurate DeepLoRa [11], the median localization error reaches up to $400\ m$ while adopting the approach in SateLoc [20], we got a median localization error of about $500\ m$. The worst localization error of those state-of-the-art models can even reach $2,000\ m$.

This localization accuracy is much worse than that reported by SateLoc [20]. The best accuracy achieved by SateLoc shows that 100% localization error is within $100\ m$ and the median localization error is $43.5\ m$ given the multi-spectral images of $50\ cm$ resolution for three gateways.

This is reasonable due to the property difference of the datasets used. On the one hand, only two gateways are deployed in our system, resulting in serious fingerprint ambiguity compared to three or more gateways. On the other hand, the localization accuracy is bounded by the resolution of cell splitting. Since the fine-grained link estimation is based on cell splitting and a cell is the smallest unit of distance comparison in our system. Therefore, a less fine-grained cell splitting can induce much higher localization errors in urban areas. For example, we compute the median localization error of 40 cells (which equals $400\ m$ since each cell is a $10\ m \times 10\ m$ area). With a similar cell-wise error, we can get a median error of $20\ m$ if we have access to remote sensing of $50\ cm$ resolution which can outperform the localization error reported by SateLoc. Thus, improving the resolution of multi-spectral images can improve localization

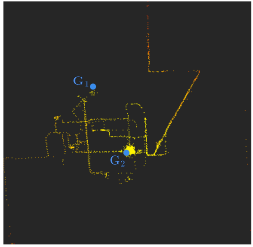


Fig. 14: Spatial distribution of the localization errors.

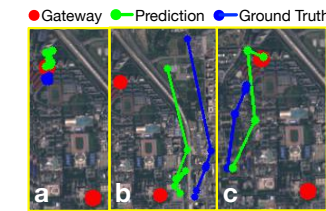


Fig. 15: Tracking different traffic trends under median localization error of 500m.

accuracy. Compared with other models, DeepLoRa achieves the best performance, consistent with the reported results [11]. Since DeepLoRa can provide more accurate ESP estimation than others, which can mitigate lots of fingerprint ambiguities. Besides, PATH/INTERSECTION has the worst performance among all approaches.

Given the two generated ESP maps for G_1 and G_2 , we further show the spatial distribution of the localization errors of DeepLoRa [11] in Figure 14. The lighter the color is, the smaller the localization error is. And the PDR reaches 0 for the black areas. An interesting observation is that the evaluated data records near G_2 have the best accuracy while it suffers from the estimated data records near G_1 . The evaluated data records far from both G_1 and G_2 have the worst localization performance. The reason has two folds. First, the ESP dynamic increases at distant locations. The ESP dynamic makes DeepLoRa hard to predict the ESP fingerprint accurately. Second, the ESP value is close to the LoRa sensitivity at long distances. The fingerprint ambiguity is increasing at many borderline areas in the whole area.

We further reduce the number of evaluated data records to see whether we can achieve a better localization accuracy when the evaluated data records are close to either G_1 or G_2 . We only select the cells whose distance from the gateway is smaller than 500 m. We use DeepLoRa to generate the two ESP map of G_1 and G_2 . Figure 13(b) shows that the data records around G_2 have more accurate localization results than those around G_1 . The reason is that the ESP observed by G_1 is much more dynamic than G_2 (Section IV-C). For G_2 , the median localization error is about 220 m. Regarding the 500 m range, it is still hard to support fine-grained localization. As shown in Figure 15, we can detect different traffic trends under current median localization of 500 m by drawing part of the trajectories of a single end node. The trends of the predicted locations almost follow the actual movement of the end node when it stays around a gateway(a), moves across the blocks, or moves towards(b)/away(c) a gateway. It is possible to apply the localization model to traffic trend prediction.

Remark. The ESP fingerprint-based localization highly depends on the granularity of the position unit, the number of gateways, and the distance to gateways. Given two gateways at 100 m^2 granularity, a sparse site survey can only achieve road-level localization for traffic trend tracking. Additionally, the dynamic nature of link ESP in urban areas degrades the

localization accuracy.

VII. OBSERVATIONS, INSIGHT, AND DISCUSSION

Observations. We deploy a LoRaWAN with two gateways and six mobile LoRa end nodes. By taking advantage of mobility, we accumulate data records that last more than 20 days to cover a large area. Moreover, we develop a mobility adaptive method to achieve the PDR estimation and coverage area calculation. Based on our link behavior study, we further verify the feasibility of fingerprint-based LoRa localization in practice. We have three key observations: 1) The temporal link behavior is much more dynamic. The main reason is the micro-environment change; 2) To obtain SNR gains of LoRa signals is an efficient way to enlarge the network coverage; 3) The localization accuracy by taking LoRa signals as the fingerprint is far from needed. It highly depends on system deployment and the granularity of site-survey.

Our Insights. We present a few key insights for the LoRa communication stack and localization method design in the future as follows:

- To deal with the link dynamics, SF 12 may not be resilient enough. We need a flexible way to extend SF to 13 or more, which is not supported on commercial-of-the-shelf LoRa radios, to avoid temporal disconnection.
- To deal with the link dynamics, the ad-hoc multiple-hop relay may be an alternative way to forward the data reliably. How to reduce the energy consumption for forwarders searching at a very low duty cycle and extra cost to maintain the network status is a critical problem.
- To obtain SNR gains in a LoRa gateway is an efficient way to enhance the coverage ability. Hence, how to detect and recover weak signals with less overhead is another important problem.
- The fingerprint-based LoRa localization suffers from the hard taming link behavior. More sophisticated techniques are needed to achieve accurate localization with narrow bandwidth and low-cost end nodes.

Measurement Universality and Deployment Diversity. With the similar settings of the LoRa transceivers, our observations may be applicable to other typical urban areas with high-density obstacles and frequent micro-environment changes as shown in Figure 3. For new areas with great disparities (e.g., rural areas, forest areas, mountain areas) from our current urban environment, the results may vary since the link behavior is highly related to the types of different land covers along the link path. The gateway siting and deployment also affect final results. A higher antenna and fewer obstacles would result in higher PDR, higher ESP, and better coverage with more LOS links.

ACKNOWLEDGEMENT

We thank the shepherd and the anonymous reviewers for their insightful comments. This study is supported in part by NSF Awards CNS-1909177.

REFERENCES

- [1] L. Alliance, "A technical overview of lora and lorawan," in <https://lora-alliance.org/resource-hub/what-lorawan>, Retrieved by July 19th 2021.
- [2] A. Research, "Nb-iot and Ite-m issues to boost lora and sigfox near and long-term lead in lpwa network connections," in <https://tinyurl.com/2026-cellular-iot>, Retrieved by July 19th 2021.
- [3] M. Centenaro, L. Vangelista, A. Zanella, and M. Zorzi, "Long-range communications in unlicensed bands: The rising stars in the iot and smart city scenarios," *IEEE Wireless Communications*, 2016.
- [4] L. SX1276, "77/78/79 datasheet, rev. 4." *Semtech*, March, 2015.
- [5] C. Li, H. Guo, S. Tong, X. Zeng, Z. Cao, M. Zhang, Q. Yan, L. Xiao, J. Wang, and Y. Liu, "Nelora: Towards ultra-low snr lora communication with neural-enhanced demodulation," in *Proceedings of ACM SenSys*, 2021.
- [6] C. Li and Z. Cao, "Lora networking techniques for large-scale and long-term iot: A down-to-top survey," *ACM Computing Surveys*, 2022.
- [7] Y. Yao, Z. Ma, and Z. Cao, "Losee: Long-range shared bike communication system based on lorawan protocol," in *Proceedings of EWSN*, 2019.
- [8] L. Mo, Y. He, Y. Liu, J. Zhao, S.-J. Tang, X.-Y. Li, and G. Dai, "Canopy closure estimates with greenorbs: sustainable sensing in the forest," in *Proceedings of ACM SenSys*, 2009.
- [9] X. Mao, X. Miao, Y. He, X.-Y. Li, and Y. Liu, "Citysee: Urban CO₂ monitoring with sensors," in *Proceedings of IEEE INFOCOM*, 2012.
- [10] S. Demetri, M. Zúñiga, G. P. Picco, F. Kuipers, L. Bruzzone, and T. Telkamp, "Automated estimation of link quality for lora: a remote sensing approach," in *Proceedings of ACM/IEEE IPSN*, 2019.
- [11] L. Li, Y. Yuguang, C. Zhichao, and Z. Mi, "Deeplora: Learning accurate path loss model for long distance links in Ipwan," in *Proceedings of IEEE INFOCOM*, 2021.
- [12] J. Yang, Z. Xu, and J. Wang, "Ferrylink: Combating link degradation for practical Ipwan deployments," in *Proceedings of IEEE ICPADS*. IEEE, 2021.
- [13] J. C. Liando, A. Gamage, A. W. Tengourtius, and M. Li, "Known and unknown facts of lora: Experiences from a large-scale measurement study," *ACM Transactions on Sensor Networks*, 2019.
- [14] J. Navarro-Ortiz, S. Sendra, P. Ameigeiras, and J. M. Lopez-Soler, "Integration of lorawan and 4g/5g for the industrial internet of things," *IEEE Communications Magazine*, 2018.
- [15] J. Haxhibeqiri, A. Karaagac, F. Van den Abeele, W. Joseph, I. Moerman, and J. Hoebeke, "Lora indoor coverage and performance in an industrial environment: Case study," in *Proceedings of IEEE international conference on emerging technologies and factory automation (ETFA)*, 2017.
- [16] J. Petajajarvi, K. Mikhaylov, A. Roivainen, T. Hanninen, and M. Petäissalo, "On the coverage of Ipwans: range evaluation and channel attenuation model for lora technology," in *Proceedings of IEEE ITST*, 2015.
- [17] J. Petäjäjärvi, K. Mikhaylov, M. Hämäläinen, and J. Iinatti, "Evaluation of lora Ipwan technology for remote health and wellbeing monitoring," in *Proceeding of the International Symposium on Medical Information and Communication Technology*, 2016.
- [18] D. Magrin, M. Centenaro, and L. Vangelista, "Performance evaluation of lora networks in a smart city scenario," in *Proceeding of IEEE ICC*, 2017.
- [19] Y. Wang, X. Zheng, L. Liu, and H. Ma, "Polartracker: Attitude-aware channel access for floating low power wide area networks," in *Proceedings of IEEE INFOCOM*, 2021.
- [20] Y. Lin, W. Dong, Y. Gao, and T. Gu, "Sateloc: A virtual fingerprinting approach to outdoor lora localization using satellite images," in *Proceedings of ACM/IEEE IPSN*, 2020.
- [21] Y. Okumura, "Field strength and its variability in vhf and uhf land-mobile radio service," *Rev. Electr. Commun. Lab.*, 1968.
- [22] M. C. Bor, U. Roedig, T. Voigt, and J. M. Alonso, "Do lora low-power wide-area networks scale?" in *Proceedings of ACM MSWiM*, 2016.
- [23] W. Xu, J. Y. Kim, W. Huang, S. S. Kanhere, S. K. Jha, and W. Hu, "Measurement, characterization, and modeling of lora technology in multifloor buildings," *IEEE Internet of Things Journal*, 2019.
- [24] A. J. Wixted, P. Kinnaird, H. Larijani, A. Tait, A. Ahmadiania, and N. Strachan, "Evaluation of lora and lorawan for wireless sensor networks," in *Proceedings of IEEE SENSORS*, 2016.
- [25] C. Li, X. Guo, L. Shuangguan, Z. Cao, and K. Jamieson, "Curvinglora to boost lora network throughput via concurrent transmission," in *Proceedings of USENIX NSDI*, 2022.
- [26] *GPS-free geolocation using LoRa in low-power WANs*. IEEE, 2017.
- [27] N. Podevijn, D. Plets, J. Trogh, L. Martens, P. Suanet, K. Hendrikse, and W. Joseph, "Tdoa-based outdoor positioning with tracking algorithm in a public lora network," *Wireless Communications and Mobile Computing*, 2018.
- [28] N. Podevijn, D. Plets, M. Aernouts, R. Berkvens, L. Martens, M. Weyn, and W. Joseph, "Experimental tdoa localisation in real public lora networks," in *Proceedings of CEUR Workshop Proceedings*, 2019.
- [29] D. F. Carvalho, A. Depari, P. Ferrari, A. Flammini, S. Rinaldi, and E. Sisinni, "On the feasibility of mobile sensing and tracking applications based on Ipwan," in *Proceedings of IEEE SAS*. IEEE, 2018.
- [30] A. Dongare, C. Hesling, K. Bhatia, A. Balanuta, R. L. Pereira, B. Iannucci, and A. Rowe, "Oopenchirp: A low-power wide-area networking architecture," in *Proceedings of IEEE PerCom Workshops*, 2017.
- [31] C. Gu, L. Jiang, and R. Tan, "Lora-based localization: Opportunities and challenges," *arXiv preprint arXiv:1812.11481*, 2018.
- [32] R. Nandakumar, V. Iyer, and S. Gollakota, "3d localization for subcentimeter sized devices," in *Proceedings of ACM SenSys*, 2018.
- [33] A. Bansal, A. Gadre, V. Singh, A. Rowe, B. Iannucci, and S. Kumar, "Owl: Accurate lora localization using the tv whitespaces," in *Proceedings of the 20th International Conference on Information Processing in Sensor Networks*, 2021.
- [34] K.-H. Lam, C.-C. Cheung, and W.-C. Lee, "Lora-based localization systems for noisy outdoor environment," in *Proceedings of IEEE WiMob*, 2017.
- [35] M. Hata, "Empirical formula for propagation loss in land mobile radio services," *IEEE Transactions on Vehicular Technology*, 1980.
- [36] H. Sallouha, A. Chiumento, and S. Pollin, "Localization in long-range ultra narrow band iot networks using rssi," in *Proceedings of IEEE ICC*, 2017.
- [37] M. Aernouts, R. Berkvens, K. Van Vlaenderen, and M. Weyn, "Sigfox and lorawan datasets for fingerprint localization in large urban and rural areas," *Data*, 2018.
- [38] W. Choi, Y.-S. Chang, Y. Jung, and J. Song, "Low-power lora signal-based outdoor positioning using fingerprint algorithm," *ISPRS International Journal of Geo-Information*, 2018.
- [39] Y. Li, Z. He, Y. Li, H. Xu, L. Pei, and Y. Zhang, "Towards location enhanced iot: Characterization of lora signal for wide area localization," in *Proceedings of IEEE UPINLBS*. IEEE, 2018.
- [40] S. Tong, J. Wang, and Y. Liu, "Combating packet collisions using non-stationary signal scaling in LPWANs," in *Proceedings of ACM MobiSys*, 2020.
- [41] Y. Liu, Y. He, M. Li, J. Wang, K. Liu, and X. Li, "Does wireless sensor network scale? a measurement study on greenorbs," *IEEE Transactions on Parallel and Distributed Systems*, 2012.
- [42] W. Dong, Y. Liu, Y. He, T. Zhu, and C. Chen, "Measurement and analysis on the packet delivery performance in a large-scale sensor network," *IEEE/ACM Transactions on Networking*, 2013.
- [43] J. Wang and W. Dong, "Understanding the link-level behaviors of a large scale urban sensor network," in *Proceedings of IEEE MSN*, 2016.
- [44] D. Aguayo, J. Bicket, S. Biswas, G. Judd, and R. Morris, "Link-level measurements from an 802.11 b mesh network," in *Proceedings of ACM SIGCOMM*, 2004.
- [45] C. K. Williams and C. E. Rasmussen, "Gaussian processes for regression," 1996.
- [46] Y. Sangar and B. Krishnaswamy, "Wichronos: Energy-efficient modulation for long-range, large-scale wireless networks," in *Proceedings of ACM MobiCom*, 2020.
- [47] C. Li, Z. Cao, and L. Xiao, "Curvealoha: Non-linear chirps enabled high throughput random channel access for lora," in *Proceedings of IEEE INFOCOM*, 2022.
- [48] A. Dongare, R. Narayanan, A. Gadre, A. Luong, A. Balanuta, S. Kumar, B. Iannucci, and A. Rowe, "Charm: exploiting geographical diversity through coherent combining in low-power wide-area networks," in *Proceedings of ACM/IEEE IPSN*, 2018.
- [49] A. Gadre, R. Narayanan, A. Luong, A. Rowe, B. Iannucci, and S. Kumar, "Frequency Configuration for Low-Power Wide-Area Networks in a Heartbeat," in *Proceedings of USENIX NSDI*, 2020.
- [50] L. Chen, J. Xiong, X. Chen, S. I. Lee, K. Chen, D. Han, D. Fang, Z. Tang, and Z. Wang, "WideSee: towards wide-area contactless wireless sensing," in *Proceedings of ACM SenSys*, 2019.

- [51] R. Nandakumar, V. Iyer, and S. Gollakota, “3D Localization for Sub-Centimeter Sized Devices,” in *Proceedings of ACM SenSys*, 2018.
- [52] F. Zhang, Z. Chang, K. Niu, J. Xiong, B. Jin, Q. Lv, and D. Zhang, “Exploring LoRa for Long-range Through-wall Sensing,” *Proceedings of ACM IMWUT*, 2020.
- [53] S. Zhang, W. Wang, N. Zhang, and T. Jiang, “RF Backscatter-based State Estimation for Micro Aerial Vehicles,” in *Proceedings of IEEE INFOCOM*, 2020.